Single and Multiple Weathering-Erosion Cycles in Supergene Ore Genesis

Paulo M. Vasconcelos
The University of Queensland, Australia

Abstract. Supergene ore deposits form when the relative tempo between weathering and erosion favors the formation and preservation of deep chemically stratified weathering profiles. If erosion outpaces weathering, weathering profiles are incipient or the surface is stripped to bedrock, and no supergene metal concentration occurs. If erosion and weathering occurs at comparable rates, metals chemically enriched at the Earth's surface are physically eroded, preventing the formation of supergene deposits. When chemical weathering is fast but chemical erosion slow, shallow weathering profiles devoid of enrichment blankets form because undesirable elements are not removed fast enough. Therefore, the ideal conditions for the formation and preservation of supergene ore deposits are relatively fast chemical weathering and erosion but slow physical erosion at the local scale, and relatively fast physical erosion, drainage incision, and lowering of the water table at the regional scale. Determining absolute ages of weathering profiles and rates of chemical and physical weathering and erosion for landsurfaces at local and regional scales is one of the primary challenges in quantifying supergene ore genesis and a necessary approach for identifying areas likely to host significant supergene ore deposits.

1 Introduction

Supergene processes (i.e., processes associated with the transport and deposition of chemical elements by meteoric water at the earth's surface) account for the formation or the economic viability of numerous ore deposits currently mined. Bauxites, channel iron deposits (CIDs), Ni-laterites, lateritic gold, and supergene manganese deposits illustrate the economic importance of weathering and erosion in ore genesis. The absolute enrichment of porphyry copper deposits or the relative enrichment of hydrothermally altered banded iron-formations improves their economic viability. In the first case, surficial processes drive ore formation; in the later, ore enrichment.

Major advances in supergene ore genesis understanding require identifying the agents (chemical vs physical, organic vs inorganic) and quantifying the processes responsible for the formation or enrichment of supergene ore deposits. A classification scheme helps to identify the nature and categorize the sequence of processes involved in the formation of particular supergene ore deposits. To quantify each process and identify major controlling factors, novel geochronological methods, cosmogenic isotope studies, and geochemical modeling are necessary.

2 Supergene Ore Genesis

Supergene ore genesis encompasses a variety of chemical and mechanical processes, often biologically mediated, that promote the concentration of a desirable mineral commodity to economic grade at the earth's surface. Chemical and physical weathering release an element of interest from its host lithology. Chemical and physical erosion separate the element of interest from gangue elements and minerals, leaving the valuable element residually enriched. Alternatively, the valuable element is physically or chemically transported to a suitable trap, where a combination of chemical, physical, or biological sedimentation promotes its re-deposition in an enriched or purified form (Figure 1).

If an element or mineral liberated by weathering processes is re-precipitated and enriched within the weathering profile, it forms an autochthonous supergene deposit (AUSD). In AUSDs, if the enrichment process occurs by the loss of relatively mobile gangue elements and minerals, where the partial or total retention of the ore element promotes an increase in its concentration with respect to the parent rock, it constitutes relative enrichment. If the enrichment process occurs by the removal of the ore element or mineral from its original site, its downward transport within the weathering profile, and its re-precipitation in concentrated grades at a lower horizon, it constitutes absolute enrichment.

If an element or mineral released from its host lithology is transported away from the original parent rock by chemical and mechanical erosion, and it is re-deposited at a distance from its source (Figure 1), it forms an allochthonous supergene deposit (ALSD). In ALSDs, the depositional process may be chemical, physical, or organic sedimentation (Figure 1). This depositional process ultimately controls the location, size, grade, and composition of the supergene ore deposit.

Finally, in the interplay between weathering and erosion, there maybe a single cycle of bedrock exposure, weathering, and supergene enrichment, forming single-cycle supergene ore deposits (SCSOD, Figure 1a). Alternatively, previously enriched profiles may be partially eroded, truncated, and re-weathered; or the eroded component may be physically transported, deposited elsewhere and re-weathered. These later scenarios characterize multi-cycle supergene ore deposits (MCSOD, Figure 1b). Distinguishing SCSODs from MCSODs is essential for differentiating among the various processes that may have contributed for the formation of an ore deposit and for determining the rates of these processes.

For example, basalts deeply weathered in situ may

form Fe-duricrusts (goethite cemented) at the surface and Al-rich duricrusts (gibbsite-cemented) between the Fe-rich horizon at the surface and a clay-rich saprolite at depth; this constitutes a single-cycle bauxite deposit. Erosion may remove the Fe- and Al-duricrusts, exposing the clay-rich horizons, depleted in iron, at the surface. Renewed weathering of the partially truncated and iron-depleted profile will preferentially remove aqueous silica, leaving a gibbsite-cemented duricrust at the surface; this constitutes a multi-cycle bauxite deposit (Figure 1b). Another example of bauxites formed by more than one cycle of weathering interrupted by an erosive event is provided in terrains where deeply weathered granites or gneisses are partially or completed eroded. During physical transport, iron oxides, quartz, and clay minerals (often kaolinite) removed from the weathered profile may be mechanically sorted and re-deposited as transported duricrusts, sand, and clay beds. Renewed weathering of clay-rich sediments will form bauxites. Deposits where more than one period of weathering are separated by a significant erosive event are MCSODs (Figure 1b).

3 Quantifying rates of weathering and erosion

Quantifying rates of weathering and erosion through time is possible trough a combination of weathering geochronology and cosmogenic isotope studies. Weathering geochronology provides ages of supergene minerals enriched in situ, or precipitated away from the source. Geochronology also permits identifying minerals that were eroded, transported, re-deposited, and partially re-weathered at the depositional site. Similarly, cosmogenic isotopes permit differentiating among minerals that formed and were continuously exposed at the Earth's surface, from minerals that formed at the surface, were eroded, transported, deposited, and re-exposed. This combination of weathering geochronology and cosmogenic isotopes is a powerful tool in unraveling the sequence of processes, and their rates through time, responsible for supergene ore genesis.

For example, dating of supergene Mn oxides and K-bearing sulfates by $^{40}Ar/^{39}Ar$ geochronology yields rates of weathering front propagation within a profile (e.g., Carmo and Vasconcelos 2006). (U-Th)/He geochronology of supergene goethite also helps quantifying rates of weathering front propagation (Heim et al., 2006; Monteiro et al. 2018). Cosmogenic ^{3}He concentrations in hematite and goethite yield long-term exposure ages for weathered profiles and supergene enrichment zones (Shuster et al. 2012; Monteiro et al. 2014, 2018a,b; Vasconcelos et al. 2019). These isotopes also permit quantifying rates of erosion for supergene deposits (Monteiro 2018a,b; Vasconcelos et al. 2019). Combining these measurements with ^{26}Al and ^{10}Be concentrations in quartz and ^{36}Cl in carbonates yield exposure ages or short-term erosion rates for the landsurfaces hosting supergene ore deposits (Vasconcelos et al. 2019). In addition, concentrations of these isotopes in sediments permit determining their depositional ages (Monteiro 2018a,b; Vasconcelos et al. 2019). Combination of these approaches at a regional scale yield timing of exposure and/or rates of weathering and erosion for exposed land surfaces, and timing of deposition and age of re-weathering of the transported material (Monteiro 2018a,b; Vasconcelos et al. 2019).

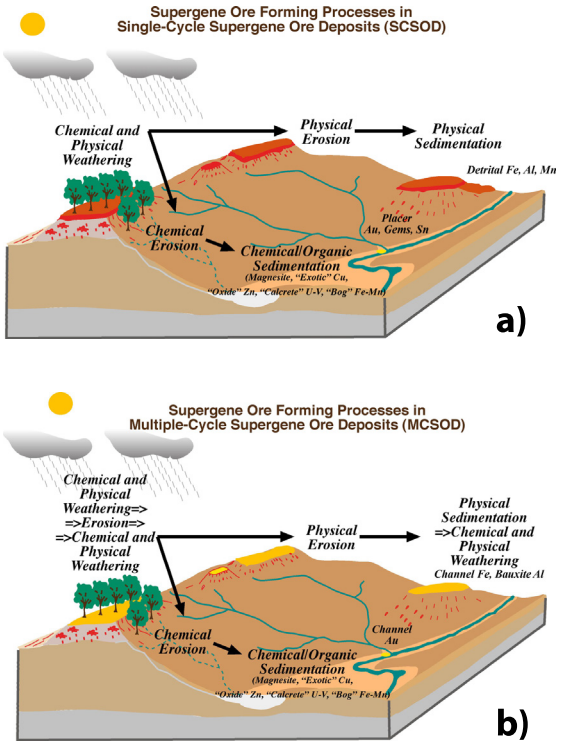

Figure 1. Diagrammatic illustration depicting the relative contributions of weathering and erosion in the formation of single-cycle vs multi-cycle supergene ore deposits.

4 Processes and rates of formation of supergene iron deposits in Brazil and Australia

Iron deposits form the largest and most valuable global mineral resources. Therefore, their genesis matters. As Brazil and Australia host the largest and richest supergene iron deposits on Earth, I concentrate on their origin by comparing and contrasting the processes and rates of formation of these deposits in these two distinct environments. The largest and most valuable iron deposits in Brazil and Australia are SCSOD formed by relative Fe enrichment during weathering of hydrothermally altered banded iron-formations (BIFs) or MCSOD formed by erosion of deeply weathered BIFs, deposition of detrital iron in aggraded rivers, and re-weathering of the detrital material to form CIDs. Supergene iron deposits in both regions result from weathering processes that initiated at least at ~80 Ma in Western Australia (Heim 2006) and ~70 Ma at Carajás (Shuster et al. 2005; Monteiro et al. 2018a), Urucum (Vasconcelos et al. 2019), and the Quadrilátero Ferrífero (Monteiro et al. 2018b). Interestingly, despite the similar

tectonic and geomorphological settings between the iron deposits in Brazil (Carajás, Quadrilátero Ferrífero, Urucum) and Australia (Tom Price, Paraburdoo), CIDs appear to only have formed in Australia.

Differences in climatically controlled relative rates of weathering and erosion likely account for the abundance of CIDs in Western Australia and their absence in Brazil. Rates of propagation of weathering fronts in Brazil were ~7–8 $m.Ma^{-1}$, while in Western Australia they were ~3-4 $m.Ma^{-1}$ during the formation of the weathering profiles. Erosion rates derived from cosmogenic isotope concentrations, on the other hand, suggest that the summits of the plateaus in Western Australia erode at a higher rate (~1 $m.Ma^{-1}$) than their counterparts in Brazil (< 0.1.Ma^{-1}) (Fujioka et al. 2010; Shuster et al. 2012; Monteiro et al. 2018a,b; Vasconcelos et al. 2019). This appears counterintuitive, as the climate in Brazil is much wetter (~1500–2500 mm average annual rainfall at Urucum, Carajas and Quadrilatero Ferrifero) than in Western Australia (~ 400 $mm.a^{-1}$). The wetter climate in Brazil promotes the formation and regeneration of resilient duricrusts, armoring the BIFs and the enriched ore deposits underneath and protecting them from erosion (Monteiro et al. 2014; 2018a,b). Vegetation and microorganisms appear to play a major role in the iron cementation that gives the duricrusts their resilience (Monteiro et al. 2014; Levett et al. 2016). In contrast, transition to arid climates in Western Australia sometime between 45–35 Ma (Vasconcelos et al. 2013) or more recently (Danisec et al. 2013) promoted the erosion of previously formed duricrusts, their deposition in aggrading river channels, and their re-weathering and iron cementation during the prolonged Neogene aridification of Western Australia. Transition from humid to arid and persistence of semi-arid to arid climates through the late Cenozoic promoted the formation and preservation of CIDs in Australia. The persistence of relatively continuous wet conditions in Brazil throughout the Neogene most likely accounts for the absence of CIDs in the iron producing regions of South America.

The approaches applied to iron deposits are also suitable in the study of the genesis of other supergene ore deposits (e.g., Vasconcelos 1999; Hautman & Lippolt 2000; Mote et al. 2001; Colin et al. 2005; Aranciba et al. 2006; Li et al. 2007; Reich et al. 2009; Deng et al. 2014; Bonnet et al. 2016;). Ongoing studies of these deposits confirm the importance of climatically controlled alternating periods of weathering and erosion in supergene ore genesis.

Acknowledgments

The author thanks the Australian Research Council for funding the $^{40}Ar/^{39}Ar$ laboratory (A39531815 and LE0882818) and weathering geochronology research at UQ (ARC DP06666925, DP160104988, LP140100805).

References

Arancibia G, Matthews SJ, Pérez de Arce C (2006) K–Ar and $^{40}Ar/^{39}Ar$ geochronology of supergene processes in the Atacama Desert, Northern Chile: tectonic and climatic relations. J. Geol. Soc. London 163:107–118.

Bonnet, NJ, Beauvais, A, Arnaud N, Chardon D, Jayananda M (2016) Cenozoic lateritic weathering and erosion history of Peninsular India from $^{40}Ar/^{39}Ar$ dating of supergene K–Mn oxides. Chem Geol 446:33–53.

Carmo IO, Vasconcelos PM (2006). $^{40}Ar/^{39}Ar$ geochronology constraints on late Miocene weathering rates in Minas Gerais, Brazil. EPSL 241:80–94.

Colin, F, Beauvais, A, Ruffet, G, Hénocque, O, (2005) First $^{40}Ar/^{39}Ar$ geochronology of lateritic manganiferous pisolites: implications for the Palaeogene history of a West African landscape. EPSL 238:172–188.

Deng X-D, Li J-W, Vasconcelos PM, Cohen BE, Kusky TM (2014) Geochronology of the Baye Mn oxide deposit, southern Yunnan Plateau: implications for the late Miocene to Pleistocene paleoclimatic conditions and topographic evolution. GCA 139:227–247.

Danisik, M, NJ Evans, ER Ramanaidou, BJ McDonald, C Mayers, BIA McInnes (2013) (U-Th)/He chronology of the Robe River channel iron deposits, Hamersley Province, Western Australia. Chem.Geol 354:150–162.

Fujioka, T, Fifield, LK, Stone, JO, Vasconcelos, PMP, Tims, SG, Chappell, J (2010) In situ cosmogenic ^{53}Mn production rate from ancient low-denudation surface in tropic Brazil, Nucl. Instrum. Meth B 268:1209–1213.

Hautmann S, Lippolt HJ (2000) $^{40}Ar/^{39}Ar$ dating of central European K–Mn oxides—a chronological framework alteration processes during the Neogene. Chem. Geol. 170:37–80.

Heim, JA, Vasconcelos, PM, Shuster, DL, Farley, KA, Broadbent, GC (2006). Dating palaeochannel iron ore by (U-Th)/He analysis of supergene goethite. Geology 34:173–176.

Levett, A, Gagen, E, Shuster, J, Rintoul, L, Tobin, M, Vongsvivut, J, Bambery, K, Vasconcelos, P, Southam, G (2016) Evidence of biogeochemical processes in iron duricrust formation, JSAES 71:131–142.

Li J-W et al. (2007) Neogene weathering and supergene manganese enrichment in subtropical South China: An $^{40}Ar/^{39}Ar$ approach and paleoclimatic significance. EPSL 256:389–402.

Monteiro, HS, Vasconcelos, PMP, Farley, KA, Spier ,CA, Mello, CL (2014) (U-Th)/He geochronology of goethite and the origin and evolution of cangas, GCA 131:267–289.

Monteiro, HS, Vasconcelos, PMP, Farley KA (2017) A combined (U-Th)/He and cosmogenic ^{3}He record of landscape armoring by biogeochemical iron cycling. JGR 123, 298–323.

Mote TI, Becker TA, Renne P, Brimhall GH (2001) Chronology of exotic mineralization at El Salvador, Chile, by $^{40}Ar/^{39}Ar$ dating of copper wad and supergene alunite. Econ Geol 96:351–366.

Reich M and 8 coauthors (2009) Supergene enrichment of copper deposits since the onset of modern hyperaridity in the Atacama Desert, Chile. Miner. Deposita 44:497–504.

Shuster, DL, Vasconcelos, PMP, Heim, JA, Farley, KA (2005) Weathering geochronology by (U-Th)/He dating of goethite, GCA 69:659–673.

Shuster, DL, Farley, KA, Vasconcelos, PMP, Balco, G, Monteiro, HS, Waltenberg, K, and Stone, JO (2012) Cosmogenic ^{3}He in hematite and goethite from Brazilian "canga" duricrust demonstrates the extreme stability of these surfaces, EPSL 329-330:41–50.

Vasconcelos, PM (1999) $^{40}Ar/^{39}Ar$ geochronology of supergene processes in ore deposits. Rev. Econ. Geol. 12:73–113.

Vasconcelos PM, Heim JA, Farley KA, Monteiro HS, Waltenberg KM (2013) $^{40}Ar/^{39}Ar$ and (U–Th)/He – $^{4}He/^{3}He$ geochronology of landscape evolution and channel iron deposit genesis at Lynn Peak, Western Australia. GCA 117:283–312.

Vasconcelos, PMP, Farley KA, Stone JO, Piacentini TL, Fifield K (2019) Stranded landscapes in the humid tropics: Earth's oldest land surfaces. EPSL in press.

Mineralogy and chemistry of Ni-phyllosilicates in the Wingellina Ni-Co laterite deposit (Western Australia): alteration processes of mafic to ultramafic lithologies

Francesco Putzolu[1], Maria Boni[1], Nicola Mondillo[1], Jens Najorka[2], Giuseppina Balassone[1], Piergiulio Cappelletti[1], Fabio S. Graziano[3], Licia Santoro[4]
[1]DiSTAR "Federico II", Napoli, Italy
[2]Core Research Laboratories, The Natural History Museum, London, UK
[3]Dipartimento di Farmacia, Università degli Studi di Napoli "Federico II", Napoli, Italy
[4]Earth Sciences Department, The Natural History Museum, London, UK

Abstract. Ni-phyllosilicates are the main phases in the saprolite zone of the Wingellina Ni-Co laterite deposit (Western Australia). In this study, we analysed the mineralogy and chemistry of the clay fraction of the saprolite from two different zones of the deposits. Our results highlight that the mineralogy, chemistry and general paragenesis of clays reflect the heterogeneity of the underlying bedrock, as well as the different alteration histories recorded in two drill cores.

The mineralogy of the saprolite zone lying on the gabbro bedrock is dominated by dioctahedral smectite clays (montmorillonite), which developed directly from the weathering of pyroxenes and plagioclases. On the contrary, the alteration of olivine resulted in the precipitation of Fe-(oxy)-hydroxides. The early stage alteration of the ultramafic unit (peridotite) involved the serpentinization of the ferromagnesian minerals. This process was followed by a Fe-(oxy)-hydroxides/quartz and smectite precipitation stage, with the latter mineral belonging both to the tri- and di-octahedral types (saponite and nontronite). The last local alteration process resulted in the formation of Ni-rich mixed-layers minerals, such as talc/smectite (T/S) and chlorite/smectite (C/S). The genesis of chlorite/smectite could be potentially due to the low temperature diagenetic process that occurred after the main lateritization phases.

1 Introduction

Mafic to ultramafic terrains weathered in tropical areas have been the subject of several studies, as their alteration produces the enrichment of metallic elements in Ni-laterite soils (Freyssinet et al. 2005; Butt and Cluzel 2013). The Ni mineralogy in laterites varies broadly and, according to such diversity, Ni-laterites have been subdivided into oxide- and phyllosilicate-types (Freyssinet et al. 2005). Oxide-type laterites are characterized by economic concentrations of Ni and Co within the ferruginous saprolite unit, in association with Fe- and Mn-(oxy)-hydroxides. Phyllosilicate-type deposits show the highest Ni-grades in the lower zones of the regolith. Nickel-bearing phyllosilicates have been the subject of several studies in past years as their mineralogy and chemistry are sensitive to the main controlling factors of the ore- and soil-forming processes: parent rock lithology and chemistry, climate, drainage, degree of hydrothermal serpentinization, chemistry of soil solutions and syn-pedogenetical tectonics. Consequently, several studies dealing with the composition and mineral transformation of phyllosilicates in soils derived from ultramafic bedrocks have been already carried out, especially where their formation is intimately related with the accumulation of Ni ores. The studies conducted on Australian ultramafic systems mainly focused on the weathering profiles in Queensland, in the Kalgoorlie district (Western Australia) and in the Murrin Murrin deposit (Western Australia). Nevertheless, there is a lack of knowledge about the pedogenesis of similar lithologies cropping out in the Musgrave Province (Western Australia), where the chemical weathering resulted in the genesis of the Wingellina laterite deposit. Here, we briefly report the results of a study on the phyllosilicates-rich horizons of the Wingellina deposit, to assess the weathering dynamics that controlled crystallographic and chemical variations during the saprolitization of the Giles Suite intrusions.

2 Geological setting

The Wingellina Ni-Co laterite deposit (Fig. 1) derived from the weathering of the olivine-rich mafic to ultramafic layered intrusion of the Mesoproterozoic Giles Complex (Putzolu et al. 2018, 2019). The weathering profile comprises an oxide-dominated zone, with high Ni and Co concentrations, and a phyllosilicate-bearing section (i.e. saprolite), which occurs as a subordinate unit. The laterite profile is characterized by a high degree of lateral variation due to the lithological heterogeneity of the magmatic bedrock, which consists of gabbro/gabbronorite and serpentinite (ex-peridotite).

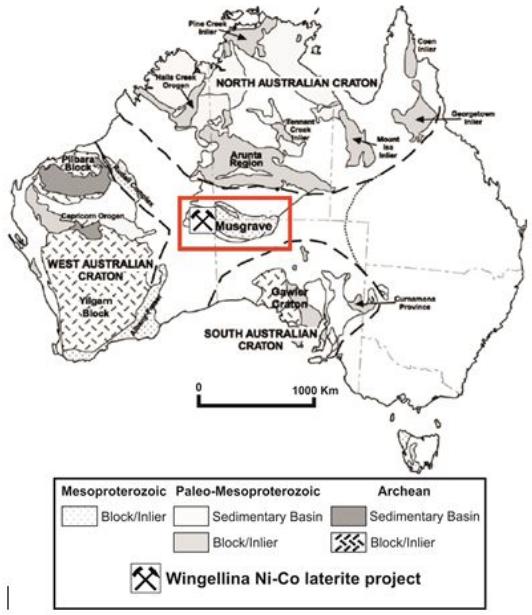

Figure 1. Tectonic map of Australia showing the location of the Wingellina deposit within the Musgrave Province area.

3 Materials and analytical methods

This study was conducted on samples collected from two saprolite zones developed from different protoliths: samples from drillcore W12 lie above a gabbro/gabbronorite bedrock, whereas samples from W19 lie on a serpentinite (deriving from the alteration of the peridotite bedrock). The specimens have been studied through X-ray powder diffraction on clay fraction (XRPD), One-dimensional X-ray diffraction modelling and Electron MicroProbe Analyses (EMPA). XRPD analyses were conducted at DiSTAR (Italy) with a Bruker D2 Phaser diffractometer. The data were acquired with a CuKα radiation of 30 kV and 10 mA. The Randomly Oriented patterns were collected at the Natural History Museum (UK) with a Panalytical X'Pert PRO MPD diffractometer equipped with an X'celerator PSD detector with a CuKα radiation, operating at 45 kV, and 40 mA. One-dimensional simulation XRPD was performed with the NEWMOD software, to assess the presence of disordered mixed layers. EMPA was performed at the NHM (UK), using a Cameca SX100 equipped with five Wavelength Dispersive Spectrometry Bragg spectrometers (beam current of 20 nA, accelerating voltage of 20 keV and a spot size of 1 µm).

4 Results

4.1 XRPD on clay aggregates

Saprolite samples from W12 (Figs 2a,b) are predominantly formed by ~15 Å to ~17 Å swelling phyllosilicates (i.e. smectites). In this drillcore, the detection of the regular sequences of the d_{001} reflections, together with the absence of systematic deviations of the d_{002}, d_{003} and d_{005} reflections of smectite in EG conditions from their overall nominal positions, suggests the presence of pure phases, rather than mixed-layer clays. The uppermost sample of W12 also contains kaolinite. The RO (Fig. 2b) patterns show that the *06l* reflections of smectite fall within a d-spacing diagnostic of dioctahedral Al-bearing smectites, in this case corresponding to montmorillonite.

Also the saprolite intersected by W19 is dominated by swelling clays (Fig. 3a), but in this unit the broadening of the d_{001} reflections of smectite and the absence of superlattice reflections and the detection of irrational d_{00l} series suggest the presence of disordered mixed-layer minerals. In addition, the typical reflections of disordered talc and serpentine occur at 10 and ~7 Å. The RO pattern (Fig. 3b) highlights the presence of both di- (d_{06l}: 1.511 Å) and tri-octahedral (d_{06l}: 1.542 Å) phases, as well as the potential occurrence of II*b* chlorite ($d_{20\text{-}4}$: 2.254 Å and d_{204}: at 2.030 Å).

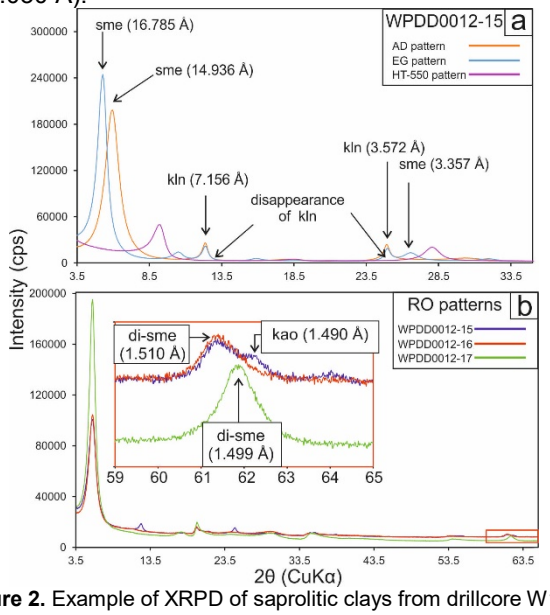

Figure 2. Example of XRPD of saprolitic clays from drillcore W12.

4.2 One-dimensional XRPD modelling

The modelling of samples from W12 showed good fitting by using a Dismectite-2Gly (d_{001}: 16.75 Å, 0.6 < Fe < 1.2, N: 1-8, delta: 4) and kaolinite (d_{001}: 7.15 Å, N: 1-30, delta: 15), occurring as discrete phases. The NEWMOD analysis showed that in a few samples from W19 the tri-smectite forms disordered mixed layers with turbostratic talc and with chlorite. The former mixed layer has been modelled with a talc/Trisme-2Gly (95–5 relative proportion, R: 0.5), whereas the chlorite-smectite mixed layer has been modelled with a di,tri-chlorite and tri-smectite structure (90–10 proportion, 1.45 < Fe < 1.75, R: 0.5). The serpentinite bedrock is characterized by the occurrence of discrete di-smectite and serpentine, modelled through Dismectite-2Gly (d_{001}: 16.7 Å, N: 1-6) and serpentine (d_{001}: 7.26 Å, N: 1-4, Fe = 1.5).

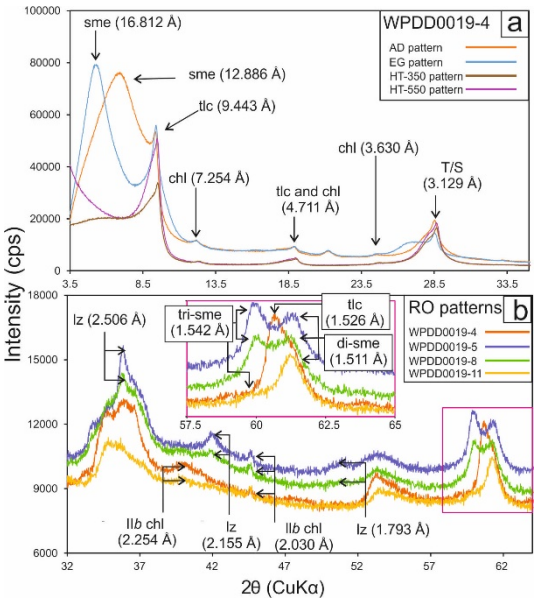

Figure 3. Example of XRPD of saprolitic clays from drillcore W19.

4.3 Textures and paragenesis

Montmorillonites in the gabbro bedrock (W12) are replacing and enclosing pyroxenes and plagioclase grains (Fig. 4a). The olivine crystals in the bedrock are not altered to phyllosilicates, but are crosscut by veins filled by Fe-(oxy)-hydroxides (Fig. 4b). The saprolite zone deriving from the gabbro bedrock is almost entirely composed of smectite, which occurs as pelitomorphic masses (Fig. 4c).

The petrographic study of the bedrock of drillcore W19 revealed a different early stage alteration style. In this drillcore the femic phases are pseudomorphed by mesh serpentines enveloping micro-aggregates of quartz and Fe-hydroxides (Fig. 4d). The uppermost section of the local saprolite is characterized by the progressive neo-formation of tri- and di-smectite that directly replaces serpentine (Fig. 4e). In their turn, tri-smectites are locally replaced by massive chlorite-smectite mixed-layers (Fig. 4e). In the uppermost section of the local saprolite, a total loss of the original magmatic texture is observed. Here, fine-grained talc-smectite is the major phyllosilicate (Fig. 4f).

4.4 Phyllosilicate mineral chemistry

Montmorillonites forming from the gabbro bedrock are close to the Al- and Fe-rich end members; starting from the bottom of the local saprolite up to its top, a general loss of Mg paired to an enrichment of dioctahedral cations (i.e. Fe and Al) has occurred (Fig. 5). The Ni gain has been observed mainly in the montmorillonites from sample WPDD0012-16 (values of 0.56 apfu).

In drillcore W19 (Fig. 6), serpentines show the lowest Ni concentrations in the local bedrock, whereas they are relatively Ni- and Fe-enriched toward the uppermost section of the saprolite (Ni up to 0.15 apfu, Fe up to 0.90 apfu). Smectitic clays with a nontronitic and saponitic chemistry are found mainly in the saprolite zone developed directly above serpentinite, with the latter showing the highest Ni concentration (up to 0.48 apfu).

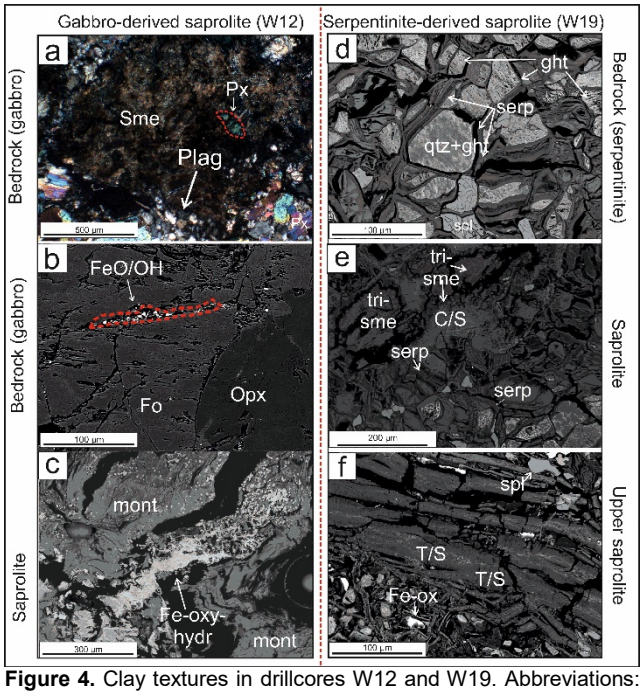

Figure 4. Clay textures in drillcores W12 and W19. Abbreviations: sme = smectite, px = pyroxene, plag = plagioclase, qtz = quartz, ght = goethite, serp = serpentine, fo = forsterite, opx = orthopyroxene, C/S = chlorite-smectite, mont = montmorillonite, T/S = talc-smectite, Fe-ox = Fe oxide, spl = spinel.

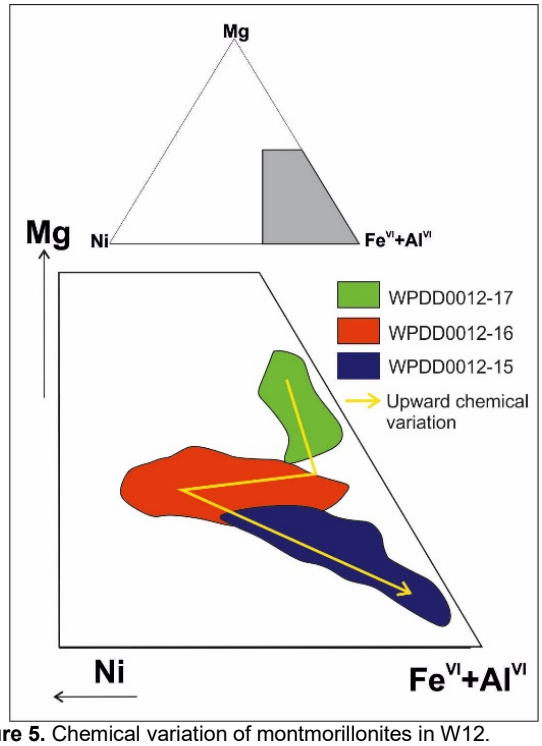

Figure 5. Chemical variation of montmorillonites in W12.

According to XRPD and NEWMOD modelling, mixed-layer chemistries have been measured mainly in the upper saprolite. Among the mixed-layer phases, the

highest Ni grades have been observed in chlorite/smectite, with Ni concentrations up to about 1 apfu, whereas talc-smectite has up to about 0.5 apfu Ni.

5 Discussion and conclusions

For the formation of thick clay units in Ni-laterites, similar to those observed at Wingellina, it is essential to have limited cation leaching as well as the existence of an impeded drainage (Gaudin et al., 2004). At the same time, the nature of the newly-formed phyllosilicates is controlled by the mineralogy of the parent rocks and by the activity of the diverse species in solution.

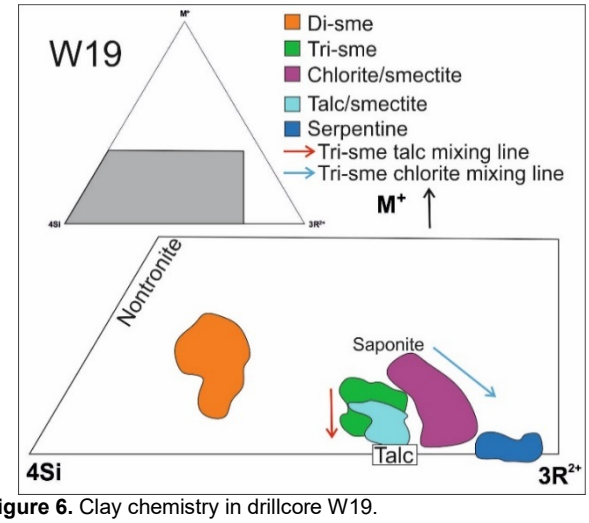

Figure 6. Clay chemistry in drillcore W19.

At Wingellina the pedogenesis of the mafic units resulted in the development of a thick secondary plasmic system, in which montmorillonite totally obliterated the original rock texture. The initial alteration stages involved the conversion of pyroxenes and plagioclases to clays, which is consistent with the observation of Eggleton (1975), whereas olivine was converted into Fe-(oxy)-hydroxides. The uppermost zone of the local saprolite is characterized also by the presence of kaolinite, which can be the result of the transformation from montmorillonite to kaolinite. This process has been widely recognized during chemical weathering, and considered a proxy for the transition from “immature” to “mature” soil systems, related to the acidification of meteoric solutions in surficial environments (Altschuler et al. 1963). The saprolitization process recorded in clay minerals observed in W19 was more complex. According to the observed paragenesis three evolutionary stages could be established:

(i) Serpentinite formation: this is the early post-magmatic alteration stage, during which olivine and pyroxenes are converted to lizardite through hydrothermal processes.

(ii) Fe-(oxy)-hydroxides/silica aggregates and smectite stage: this is the first weathering stage, in which Fe-(oxy)-hydroxides and silica formed as pseudomorphs of the still unaltered olivine. This process commonly represents the initial stage of the ferralitic alteration at tropical latitudes (Delvigne et al. 1979). Concurrent with the FeO/OH+quartz formation, oxidative weathering resulted in Mg leaching from serpentine and Ni gaining in neo-formed tri- and di-smectite (Hseu et al. 2007). Although no textural association between di- and tri-smectites has been detected, it is possible to infer that Fe-rich smectite formed from the transformation of Mg(Ni)-smectite due to a local increase of the drainage conditions and of the leaching degree.

(iii) Mixed-layers stage: mixed-layers were identified either as overprints on tri-smectite (as chlorite/smectite) or as total replacements of serpentinite textures, thus highlighting that their formation was linked to late stage processes during saprolitization. The late precipitation of C/S and T/S could reflect a local post-lateritization process resulting from low temperature diagenesis and/or authigenic processes (Beaufort et al. 2015).

Acknowledgements

This contribution is part of the ongoing PhD of Francesco Putzolu at the DiSTAR. The authors are indebted to Max Maczurad (Metals X Ltd.) for field assistance and to John Spratt (Natural History Museum of London, UK) for technical help during EMPA analyses. This study has been funded by “Programma per il finanziamento della ricerca di Ateneo 2016 -Progetto CEB”, granted by Università degli Studi di Napoli Federico II (Italy) to Dr. Nicola Mondillo.

References

Altschuler ZS, Dwornik, EJ, Kramer, J (1963) Transformation of montmorillonite to kaolinite during weathering. Science 141:148–152.

Beaufort D, Rigault C, Billon S, Billault V, Inoue A, Inoue S, Patrier P (2015). Chlorite and chloritization processes through mixed-layer mineral series in low-temperature geological systems–a review. Clay Miner 50(4):497–523.

Butt CR, Cluzel D (2013) Nickel laterite ore deposits: weathered serpentinites. Elements 9(2):123–128.

Delvigne J, Bisdom EBA, Sleeman J, Stoops G (1979). Olivines, their pseudomorphs and secondary products. Pedologie 29(3):247–309.

Eggleton RA (1975). Nontronite topotaxial after hedenbergite. Am Mineral: Journal of Earth and Planetary Materials 60(11-12):1063–1068.

Freyssinet P, Butt CRM, Morris RC, Piantone P (2005). Ore-forming processes related to lateritic weathering. Econ Geol 100th anniversary volume, 681–722.

Gaudin A., Grauby O, Noack Y, Decarreau A, Petit, S (2004). Accurate crystal chemistry of ferric smectites from the lateritic nickel ore of Murrin Murrin (Western Australia). I. XRD and multi-scale chemical approaches. Clay Miner 39(3):301–315.

Hseu ZY, Tsai H, Hsi HC, Chen, YC. (2007). Weathering sequences of clay minerals in soils along a serpentinitic toposequence. Clays and Clay Miner, 55(4):389–401.

Putzolu F., Balassone G, Boni M, Maczurad M, Mondillo N, Najorka J, Pirajno F (2018). Mineralogical association and Ni-Co deportment in the Wingellina oxide-type laterite deposit (Western Australia). OGR 97:21–34.

Putzolu F, Boni M, Mondillo N, Maczurad M, Pirajno F. (2019). Ni-Co enrichment and High-Tech metals geochemistry in the Wingellina Ni-Co oxide-type laterite deposit (Western Australia). J Geochem Expl 196:282–296.

New data on the Francevillian manganese ore from Bignomi plateau, Gabon

Alexis NDONGO, Norbert ONDO ZUE ABAGA, Benjamin MUSAVU MOUSAVOU, Simplice M. NDONG ONDO
Université des Sciences et Techniques de Masuku, Département de Géologie, Franceville, Gabon

Kalle KIRSIMAE
University of Tartu, Geology department, Tartu, Estonia

Abstract. Manganese deposits in the Franceville basin have largely been studied thanks to the discovery and exploitation of worldclass manganese ore of Bagombe. The results from these studies on the Bagombe plateau are commonly generalized to all deposits in the Franceville basin. We present here new data from Bignomi deposit located in the south of the basin. As in Bangombe, the profile shows five horizons of massive ore (H1), platy ore (H2), transition layer (H3), pisolite (H4) and humic layer (H5). However, unlike in Bangombe where the most enriched layer is H2, the high grade horizon (44% Mn) in Bignomi is the Massive horizon (H1). This Mn enrichment of the lower part of the profile could be linked to the karstic and fractured system which allowed Mn-rich fluids to flow in channels towards the lower horizons. That is showed by the occurrence of manganese oxides in fractures, cavities and pores. Furthermore, X-ray diffraction (XRD) reveals that material from massif Horizon (H1) consists of a mixture of different poorly crystalline Mn-oxyhydroxides which were impossible to quantify. This result suggests that the massif horizon of the Bignomi deposit can be considered, unlike in Bangombé, as a recently precipitated material.

1 Context of the study

Manganese deposits in Franceville basin have been known since the 19th century (Barrat 1895). Previous work carried out in the basin since the 1960s has highlighted several manganese rich plateaus located in Moanda, Franceville and Okondja. These include, Bagombe, Okouma, Bafoula and Yeye in Moanda area and Menai, Bordeau, and Biniomi in Franceville (Weber 1969; Pambo 2004).

Bagombe plateau contains the largest manganese deposit in Franceville basin evaluated at 20 million tons before exploitation. This deposit has been in operation for some 30 years by the COMILOG Company owned by Eramet group.

Located southeast of the Franceville city, the Biniomi plateau contains one of the minor manganese deposits in the basin. This deposit is currently operated by Nouvelle Gabon Mining Company and has been estimated at 35 million tons. As Bignomi deposit is of small importance compared to Bagombe, it has not been the subject of any scientific study to date.

The numerous scientific studies carried out on the manganese deposits in Bagombe plateau, have made it possible to establish a synthetic log of the mineralized layer, to identify mineralizations types and to know the geochemical and metallogenic composition of the deposit (Bouladon 1963; Weber 1969; Azzibrouck Azzilet 1986; Pambo 2004).

Studies on the Bagombe plateau have often been generalized in Franceville deposits, but smaller deposits must also be studied in order to better constrain the paleogeochemical and paleoclimatical processes that led to manganese accumulation in the basin.

We have been working since 2017 on the Bignomi deposit with the aim of understanding the geological and paleoatmospheric evolution of manganese precipitation in the protore, to characterize the mineralogical core and to determine the geochronological age of the manganese enrichment of the deposit.

We present here preliminary results obtained by meso to microscale studies of manganese profile as well as bulk XRD, XRF analysis and SEM mapping of two samples (Bi01 and Bi02) from massive horizon (H1) of Bignomi deposit. XRD, XRF and SEM mapping where performed at the Universty of Tartu in Estonia.

2 Geological background

Bignomi deposit is located in the eastern part of the Franceville basin. This basin was opened during the Paleoproterozoic as an intracratonic basin. The opening of the basin was led by two major fault sets such as (1) N–S-transverse faults and (2) longitudinal normal faults that run parallel to the overall NW–SE trend of the basin. Those faults combined to open the Franceville basin (Gauthier-Lafaye, 1986; Pambo et al., 2006; Bouton et al., 2009a, Ndongo et al., 2016)

The Franceville Basin has been extensively studied thanks to the discovery and exploitation of worldclass manganese resources (Pambo 2004) and uranium deposits (Weber 1969). This basin which lies in the Haut Ogooué region of south-eastern Gabon, is hosted by the Francevilian series. The stratigraphic column of the Francevillian series has been defined into five stratigraphic units FA, FB, FC, FD, and FE (Weber 1969), arranged into two sedimentation cycles (Parize et al., 2013). The FA (Francevillian A) forms the base of the series which is made up of coarse sandstones and conglomerates interbedded between pelitic layers at the base and the alternating coarse to medium sandstones and silt-sandstones toward the top. According several

authors, the FA formation could correspond to a large Paleoproterozoic delta system (Gauthier-Lafaye 1986; Pambo et al., 2006; Deynoux and Duringer 1992; Ndongo et al., 2016). The FB (Francevillian B) is made up mostly of marine black shales and organized into two stratigraphic subunits, FB1 and FB2 (Weber 1969). The FB1 subunit is mainly composed of black shales with dolomite and manganese rich layers in the upper part (Weber 1969; Azzibrouck Azziley 1986; Gauthier-Lafaye 1986; Pambo 2004). The FB2 is about 100 meters thick and is made up mostly of Poubara sandstones (FB2a) and black shales (FB2b) which have been associated with turbidites (Parize and al., 2013). The FC (Francevillian C) comprises massive dolomites, ribbon chert, and stromatolithic jaspes. The following Formations FD and FE (Francevillian D-E) are prominent in the northern part of the Franceville Basin and in the Okondja Basin (Bouton et al., 2009a), but they are poorly documented in terms of their depositional environments. FD-FE are composed of black shales and sandstones associated with volcano-sedimentary deposits (Weber 1969 Gauthier-Lafaye and Weber 1989; Thiéblemont et al., 2014).

The first geochronological data have shown that the Francevillian group formed between c. 2100 and 2000 Ma (Ruffenach et al., 1976; Bros et al., 1992; Horie et al., 2005) but the youngest age reported on zircon from FA and FB around Ngoutou volcanic complex, is 2191± 13 Ma (Sawaki et al., 2016).

3 Manganese deposits in Franceville basin

Manganese deposits in the Franceville basin form a superficial layer that outcrops in several plateaus (Bagombe, Okouma, Bafoula, Menai-Oyali, Bordeau, Biniomi) at 600 meters altitude around Moanda, Franceville and Okondja cities (Weber 1969; Pambo 2004). Bagombe plateau is the most important deposits with 19 km^2 and 200 million of tones before exploitation. This deposit is still exploited by the COMILOG Company and constitutes the base of all studies done on the manganese in Franceville basin.

The synthetic log of the manganese profile described on the Bagombe plateau has five main horizons, including mineralized base layers topped by a humic horizon. This profile rests on the manganese hosted black shales (FB1) with manganese content varying between 5 and 30% (Weber 1969; Pambo 2004). These manganous black shales are considered to be the protore of the deposit. Several authors have shown that the mineralization of the Bagombe plateau is the result of the meteoric weathering process which has led the replacement of manganous carbonates (Mg, Ca, Mn)CO_3 by manganese oxide/hydroxide, on the manganese-rich black shales (Bouladon et al., 1965; Weber 1973; Nziengue Mapangou 1981; Beauvais 1984; Azzibrouck Azziley 1986; Pambo 2004).

4 The Manganese deposit of Bignomi plateau

The Bignomi manganese deposit is located in the south-east of Franceville city, in a landscape of a succession of hills varying sizes along West-East trend. Bignomi plateau is part of deposits acquired by the Nouvelle Gabon Mining Company which exploited the plateau since 2017.

4.1 Synthetic log of the Bignomi deposit

The studied profile is about 5 meters thick with lateral extension exceeding a hundred meters. It rests directly on the black shales attributed to the top of FB1 (Francevillian series). We have identified five horizons in Bignomi plateau (H1, H2, H3, H4, and H5). According to the data from the Company, manganese content in the profile ranges from 35% at the base of the profile (H1) to less than 10% at the top (H5).

Massive horizon (H1) is directly in contact with FB1 black shales. This horizon is manly made up of a massive manganous layer (30-40% Mn). Massive layer evolves laterally toward complex forms including cavities, stalactites or lens concretions. **Platy horizon (H2)** overlies the massive horizon and is mainly composed of platies associated to clay with 25 to 30% Mn content. Careful analysis of this horizon showed that platies are randomly distributed in the horizon and are affected by fractures which are filled or not by manganese oxides. **Transition horizon (H3)** rests on platy level. Its thickness varies between 0.1 and 0.5 meters. This horizon is formed by a mixture of pisolites and platies. **Pisolite horizon (H4)** is mainly composed of pisolites of variable sizes. The upper part of the horizon is constituted of massive blocks of pisolite aggregates. **Humic horizon (H5)** is made of soil rich in clays and sandstones including some pisolites (<10% Mn), where vegetation develops.

4.2 Litho-geochemical description of the Massive horizon of Bignomi deposit

Detailed study of the massive horizon (H1) reveals that the ore is associated with variying sized cavities where Mn features as lenticular, botryoidal and stalactite shapes. Cavities are usually coated by manganese oxides. Small scale botryoidal bodies are associated with lens and stalactite shape in the cavities.

Two samples were respectively taken on stalactite shapes (Bi01) and crust covered cavities (Bi02). Those samples were analyzed by XRD, XRF and SEM mapping at the University of Tartu (Estonia). XRF shows that Bi01 and Bi02 samples are mainly made of Mn oxides ranging from 43 to 44 %. Manganese oxides are associated with several other oxides such as SiO_2 (5 -8%), Al_2O_3 (7%), Fe_2O_3 (<1%). Other elements like Ca, K, Ti, P, S, occur as traces. These results demonstrate that the high grade manganese horizon is the massive horizon, which is different in Bagombe where the platy horizon holds the highest Mn content (Azzibrouck Azziley 1986; Pambo 2004). XRD reveals that material from massif Horizon (H1) consists of a mixture of different poorly crystalline Mn-oxyhydroxides which were impossible to quantify. This result suggests that the massif horizon of Bignomi deposit can be considered as a recently precipitated material, they are either amorphous or too finely

crystalline to produce a discernible diffraction pattern via XRD (Zhang and Karathanasis 1997; Johnson et al., 2016).

SEM imaging was obtained on a polished cross section (2.5 cm wide) of a stalactite manganese concretion (Bi01 sample). As shown by Fig. 1a, this concretion consists of dark gray small scale concretions embedded in the light grey matrix. However, there is no significant distinction between concretions and matrix in terms of texture and composition (Fig. 1d, e). Texture is mainly porous with small cavities randomly distributed in the section (Fig. 1d, e). EDS element map shows a typical composition of Bi01 sample made of Mn, Al, Si and Fe which are distributed according to the texture. As shown in EDS element map (Fig.1), Mn and Al, the main phases, are abundant in the vicinity of pores and cavities. This particular distribution is probably the result of Mn and Al rich fluids circulation and subsequent precipitation within the pores and cavities (Zhang and Karathanasis 1997).

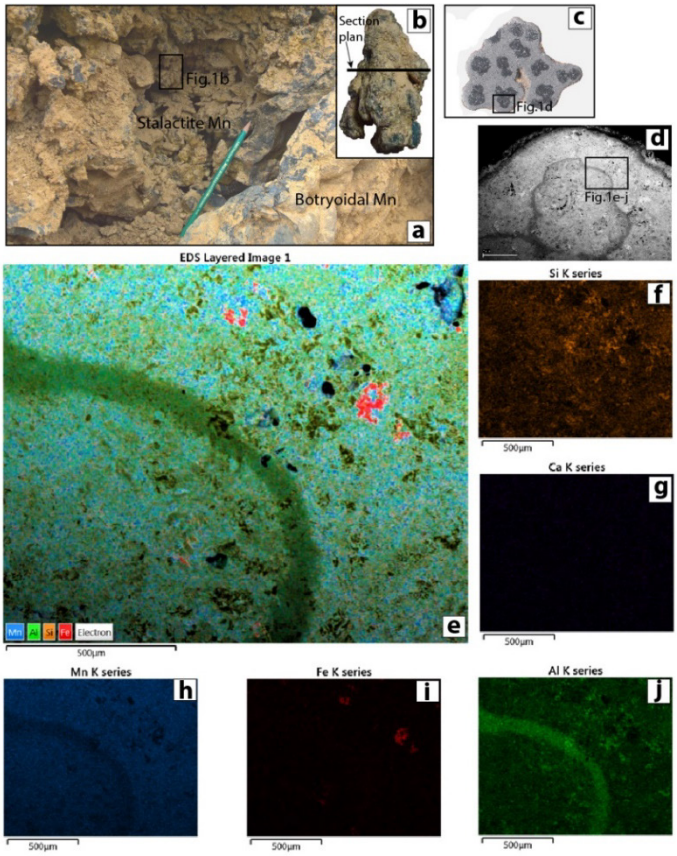

Figure 1. Lithological and geochemical features of Manganous concretions of Bignomi deposit (Franceville basin). a) Massive horizon picture showing botryoidal and stalactite Mn ore, b) macro-scale picture concretion with section plan, c) SEM image of stalactite cross-section, d-j) EDS map of fig.1.d selected area.

Massive Horizon (H1) also displays two fracture types which cut through the massive ore. They are completely filled by manganese oxide or not. When not completely sealed, the fractures sides are often covered by manganese oxides.

We therefore suggest that Mn enrichment of Massive horizon of Bignomi deposit is linked to the karstic and fracture system which allowed Mn-rich fluids to flow channels toward the lower horizons. That is shown by the occurrence of manganese oxides in fractures, cavities and pores.

Acknowledgements

We are grateful for manuscript comments and analytical support the University of Tartu all of those who has contributed in this study. We acknowledge Nouvelle Gabon Mining Company which allows us to work and sample in Bignomi open pit.

References

Azzibrouck-Azziley, G., 1986. Sédimentologie et géochimie du Francevillien B (Pro-térozoïque inférieur). Métallogénie des gisements de Manganèse de Moanda, Gabon. Thèse de Doctorat du 3eme cycle. Université de Strasbourg, 214 p.

Barrat, M. (1895). *Sur la géologie du Congo français*. C. Dunod & P. Vicq.

Beauvais, A. (1984). Concentrations manganésifères latéritiques : étude pétrologique de deux gîtes sur roches sédimentaires précambriennes: gisements de Moanda (Gabon) et d'Azul (Brésil) *(Doctoral dissertation).*

Bouladon M., 1963. Le gisement de manganese de Moanda (Gabon). Etude de la premiere exploitation. Rapport BRGM n°5313/MPMG

Bouton, P., Thiéblemont, D., Simo Ndounze, S., Goujou, J.C., Kassadou, A.B., Walemba, A., Boulingui, B., Ekogha, H., Moussavou, M., Lambert, A., Roberts, D., Deschamps, Y., Préat, A., 2009a. Carte géologique de la République du Gabon à 1/200 000, feuille Franceville – Boumango. Editions DGMG – Ministère des Mines, du Pét-role, des Hydrocarbures, Libreville.

Bros, R., Stille, P., Gauthier-Lafaye, F., Weber, F., Clauer, N., 1992. Sm\Nd isotopic dat-ing of Proterozoic clay material: an example from the Francevillian sedimentaryseries Gabon. Earth Planet. Sci. Lett. 113:207–218.

Deynoux, M., Duringer, P., 1992. Etude sédimentologique du gisement d'uraniumd'Oklo et d'Okélobondo. Protérozoïque inférieur de bassin de Franceville, Gabon.Rapport interne CNRS. Centre de Géochimie de la Surface, Institut de Géologie àStrasbourg, pp. 35.

Gauthier-Lafaye, F., 1986. Les gisements d'uranium du Gabon et les réacteursd'Oklo.Modèle métallogénique de gîtes à fortes teneurs du Protérozoïqueinférieur.Thèse de Doctorat d'Etat. Université de Strasbourg, Mémoires SciencesGéologiques 78:250.

Gauthier-Lafaye, F., Weber, F., 1989. The Francevillian (Lower Proterozoic) uraniumore deposits of Gabon. Ecol. Geol. 84:2267–2285.

Horie, K., Hidaka, H., Gauthier-Lafaye, F., 2005. U-Pb geochronology and geochem-istry of zircon from the Franceville series at Bidoudouma, Gabon. Geochim.Cosmochim. Acta 69 (10):A11.

Johnson J. E., Webb S. M., Ma C., Fischer W. W., 2016. Manganese mineralogy and diagenesis in the sedimentary rock record, *Geochimica et Cosmochimica Acta 173 (2016):210–231.*

Ndongo, A., Guiraud, M., Vennin, E., Mbina, M., Buoncristiani, J.F., Thomazo, C., Flotté, N., 2016. Control of fluid-pressure on early deformation structures in the Paleoproterozoic extensional Franceville Basin (SE Gabon). Precambr. Res. 277, 1–25.

Nziengui-Mapangou, P. (1981). Pétrologie comparée de gisements manganésifères supergènes en Afrique (gisement de Ziémougoula, en Côte d'Ivoire et gisement de Moanda, au Gabon). *Thesis of University of Poitiers, Poitiers*.

Parize, O., Feybesse, J.L., Guillocheau, F., Mulder, T., 2013. Were the 2.1-Gyr fos-sil colonial organisms discovered in the Francevillian Basin (Palaeoproterozoic, Gabon) buried by

turbidites? Comptes Rendus Geosci. 345 (2):101–110.
Pambo, F., 2004. Condition de formation des carbonates de manganèse protéro-zoïques et analyse minéralogique et géochimique des minerais à bioxydes demanganèse associés dans le gisement de Moanda, (Sud-Est, Gabon). Unpub-lished thesis of Université de Bourgogne, 274 pp.
Pambo, F., Guiraud, M., Quesne, D., Gauthier-Lafaye, F., Azzibrouck, G., Lang, J., 2006.The Proterozoic Franceville Basin (SE Gabon): an example of interaction betweenmarine sedimentation and extensional faulting. Afr. Geo. Rev. 13:77–106.
Ruffenach, J. C., Menes, J., Devillers, C., Lucas, M., & Hagemann, R. (1976). Etudes chimiques et isotopiques de l'uranium, du plomb et de plusieurs produits de fission dans un échantillon de minerai du réacteur naturel d'Oklo. *Earth and Planetary Science Letters*, *30*(1):94-108.
Sawaki, Y., Moussavou, M., Sato, T., Suzuki, K., Ligna, C., Asanuma, H., & Edou-Minko, A. (2017). Chronological constraints on the Paleoproterozoic Francevillian Group in Gabon. *Geoscience Frontiers*, *8*(2):397-407.
Thiéblemont, D., Castaing, C., Billa, M., Bouton, P., Préat, A., 2009. Notice explicativede la Carte géologique et des Ressources minérales de la République gabonaiseà 1/1,000,000. Editions DGMG – Ministère des Mines, du Pétrole, des Hydrocar-bures, Libreville, 384 p.
Weber, F., 1969. Une série précambrienne du Gabon: le Francevillien. Sédimentolo-gie, géochimie, relations avec les gîtes minéraux associés PhD., 28. UniversitéLouis Pasteur and Memoire Service Cartes Géologique Alsace-Lorraine, Stras-bourg, France, 328 p.
Weber, F. (1973). Genesis and supergene evolution of the Precambrian sedimentary manganese deposit at Moanda (Gabon). *Genesis of Precambrian Iron and Manganese Deposits*, 307-322.
Zhang M., Karathanasis A. D., 1997. Characterization of iron-manganese concretions in Kentucky alfisols with Perched Wter Tables, *Clays and Clay Minerals,* 45(3):428-439.

Characterisation of the nonsulphide zinc ore at Huoshaoyun, Northwestern China, and its genetic aspects

Wenbin Jia, Fengyue Sun
College of Earth Science, Jilin University, China

Guangsheng Yan
China Geological Survey, Beijing, China

Abstract. The Huoshaoyun carbonate-hosted nonsulfide Zn deposit, in the Sanjiang-Tethys metallogenic belt of west China, is a newly discovered world-class deposit. Two ore bodies occur in the Longshan Formation limestone, in which the ore textures are mainly developed as laminated, banded, and brecciated. The metal minerals of the Huoshaoyun deposit are dominated by smithsonite and cerussite, with subordinate amounts of galena and siderite. Ore mineralization of this deposit is distinguished into three stages: sulfide stage, oxidation stage, and post-oxidation stage. Unlike most supergene Zn-Pb deposits, the Huoshaoyun orebody shows comparable ore grades for both Pb and Zn with an inverse supergene chemical zoning. Zinc is most abundant at the top of the deposit, whereas lead increases with depth. These two elements have different mobilities in solution, which implies that the primary source of zinc in the Huoshaoyun nonsulfide mineralization was originally located not far from the primary galena mineralization, the remnants of which are present in situ. Supergene zinc mineralization was derived from the dissolution of primary sphalerite hosted in the now-eroded rocks above the Huoshaoyun mine site. Zinc-rich solution migrated through the sedimentary host rocks, precipitated Zn minerals in pore spaces, and replaced detrital and hydrothermal alteration minerals.

1 Introduction

The Himalayan-Zagros orogenic system (Fig. 1), which formed by the India-Eurasia and Arabia-Eurasia collisions, is a classic example of a young and active continent–continent collisional orogenic system (Yin and Harrison 2003; Spurlin et al. 2005; Hou et al. 2011). The system hosts a world-class polymetallic metallogenic province that extends along strike for 10,000 km and includes some carbonate-hosted Pb-Zn deposits. Among them, clusters of Zn-Pb mineralization occurring in the Sanjiang-Tethys Belt of the Tibetan Plateau in China (Hou et al. 2008; Deng et al. 2014b; Deng and Lin 2015), and the Sanadaj-sirjan Zone in Iran (Rajabi et al. 2012; Mirnejad et al. 2011).

The Huoshaoyun is a newly discovered world-class Zn-Pb deposit located in the west Sanjiang Belt. The deposit (with more than 19.6 million tons of Zn+Pb at grades of 23.6% Zn and 5.6% Pb) (unpublished data) is the largest known and the only currently mined deposit in China (Dong et al. 2015). Moreover, Huoshaoyun is the first discovered nonsulfide deposit in China, and study of the nonsulfide Zn deposit is still a blank space in China.

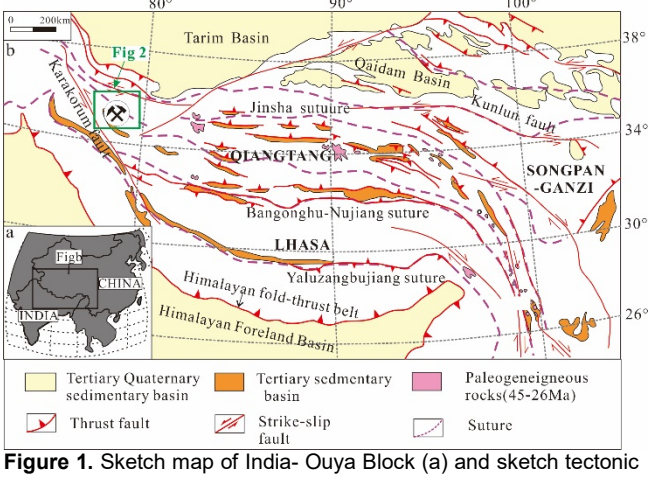

Figure 1. Sketch map of India- Ouya Block (a) and sketch tectonic map of the Tibetan collision belt and locations of the study zones (b). After Spurlin et al. (2005).

2 Ore deposit geology

The Huoshaoyun deposit is situated in the southern part of the Tianshuihai basin, which lies in the west of the Sanjiang-Tethyan Metallogenic Belt. The Proterozoic metamorphic basement (Tianshuihai Group) consists mainly of metasandstone, phyllite intercalated with limestone, and unconformably overlain by Paleozoic strata. The Paleozoic and Mesozoic strata includes seven formations: Qiaoerti, Kongkashan, Heweitan, Keleqinghe, Longshan, Hongqilapu, and Tielongtan (Fig. 2). Mineralization is hosted by the Longshan Formation, which consists of bioclastic limestone and sandstone. The Longshan Formation includes four members: (1) the lower member consists of thick sandstone (~100 m thick), (2) the middle member hosting the ore-bodies, consists of micrite and bioclastic limestone (100~200 m thick), (3) the middle member consists of mudstone and argillaceous rocks (50~200 m thick), (4) the upper member containing metal mineralization, consists of limestone (20~300 m thick). All the mineralization occurred in the carbonatite and extended stably in the Huoshaoyun deposit area.

The fault structures in the area are simple. The NEE trending fault (F10, F11) and NWW trending fault (F6) are normal faults, which dislocated the ore bodies and strata (Fig 3). The ore-controlling regional structures in the mine area are the Qiaoertianshan fault, the Heweitan fault and their secondary faults (Fig. 3).

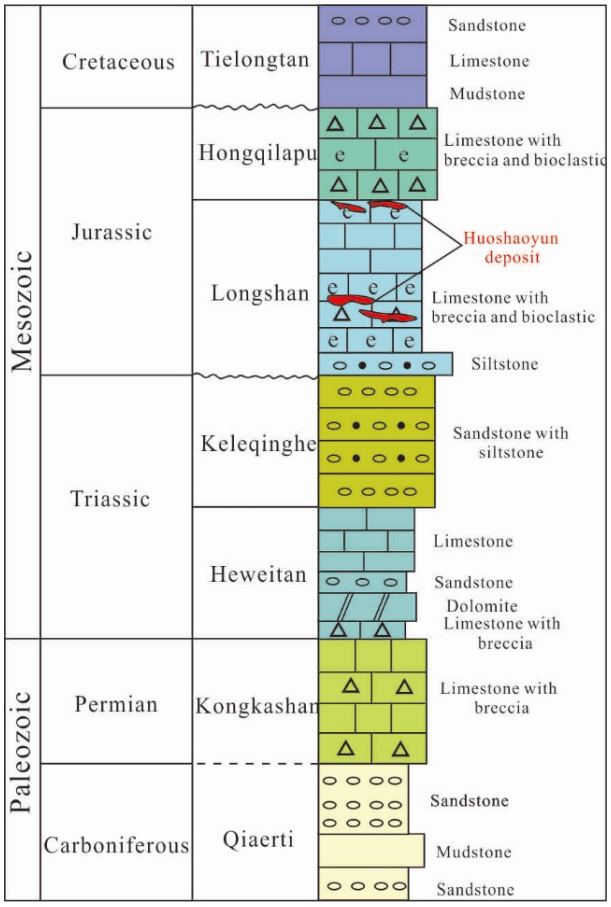

Figure 2. Stratigraphic column showing the position of carbonate-hosted Zn-Pb mineralization in the Huoshaoyun deposit. Orebodies of the Huoshaoyun deposit are hosted in the Longshan Formation limestone.

2.1 Ore body

According to the pattern of distribution and position, the ore bodies can be divided into two sections: no. II and III (Fig. 3). These two orebodies are developed nearly parallel, the average grade of Zn and Pb is 23.6% and 5.7%, respectively. No. II ore body is about 260 m long, 160 m wide, and located in the upper part of the fourth member of Longshan formation. The No. III ore body is the main mineralized layer, which is located in the second member of the Longshan formation. The ore body is about 2280 m long, 1400 m wide and 25~55 m high, which is controlled by the carbonate.

Orebodies in the Longshan Formation mainly occur as laminated, banded, and brecciated ores. The metal minerals of the Huoshaoyun deposit are dominated by smithsonite and cerussite, with subordinate amounts of galena and siderite. The gangue minerals comprise calcite, dolomite and gypsum. Due to the content of Fe and Mn, smithsonite of different colors, such as brown, reddish and light-brown, can appear in the same stratum and thin section. The cerussite is mainly white, with massive, layered and brecciated structure.

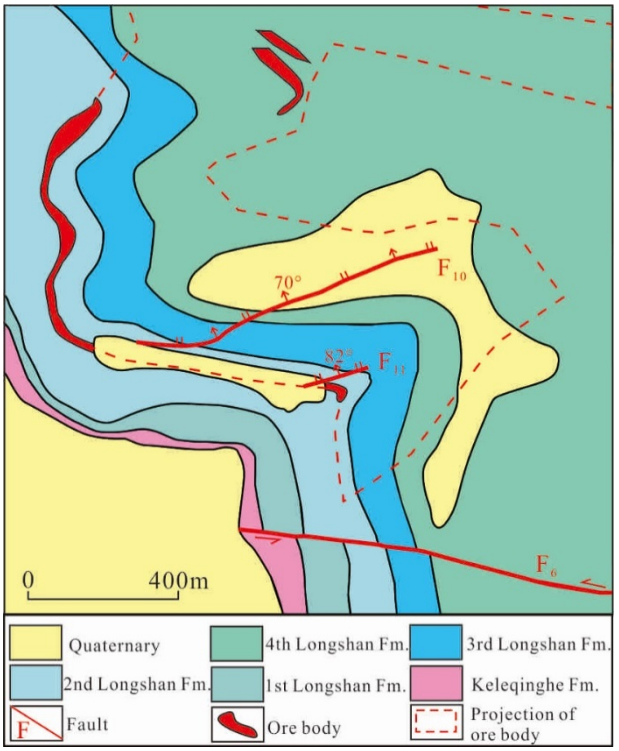

Figure 3. Simplified geological map of the Huoshaoyun deposit

The tectonic system not only provides a migration pathway for ore-forming fluids, but also provides room for the formation of the ore deposits. The ore bodies developed in the southern Tuofengshan-Bilongtan inverted syncline. The axis of this syncline is NW-trending, about 120 km long and 30 km wide. The strata in the core are the Hongqilapu formation, and the Fold limbs expose the Longshan formation and Triassic stratum. The Huoshaoyun deposit is stratabound within the Longshan formation of the southern limb of syncline.

2.2 Mineralization stages

Based on the mineral paragenetic association of the deposit, three stages of hydrothermal mineralization are established (Fig. 4).

Mineral	Sulfide stage	Oxidation stage	Post-oxidation stage
Pyrite			
Sphalerite			
Galena			
Simithsonite			
Anglesite			
Iron oxides			
Cerussite			
Hydrozincite			
Gypsum			
Calcite			

Figure 4. Paragenetic sequence for minerals in the Huoshaoyun Zn-Pb deposit.

Sulfide stage: A number of metallic sulfides were developed in this stage, such as pyrite, galena, and

sphalerite (Fig. 5a). At present, galena is commonly rimmed by anglesite that contains abundant sub-size galena inclusions (Fig. 6a). Anglesite forms an armour around galena, protecting it from direct contact with oxidising reagents (Fig. 6b).

Oxidation stage: this stage is a subordinate economic stage characterized by breccia matrix composed of disseminated cerussite and minor smithsonite (Fig. 5b). Black cerussite contains abundant relics of galena (Fig. 5c). The smithsonite precipitates as massive botryoidal layers (Fig. 5d) or as a fine-crystalline matrix of carbonate breccia in the limestone host rocks (Fig. 6c and 6d).

Post-oxidation stage: the main economic stage, consisting of white cerussite, smithsonite, hydrozincite and anglesite. The purest nonsulphide zinc ore, locally referred to as "calamine", has formed typically at the uppermost levels of the carbonate rocks by rhythmic replacement of cerussite and as joint fillings (Fig. 5e and 6e). In addition, some of the cerussite aggregated as the massive ore (Fig. 5f and 6f).

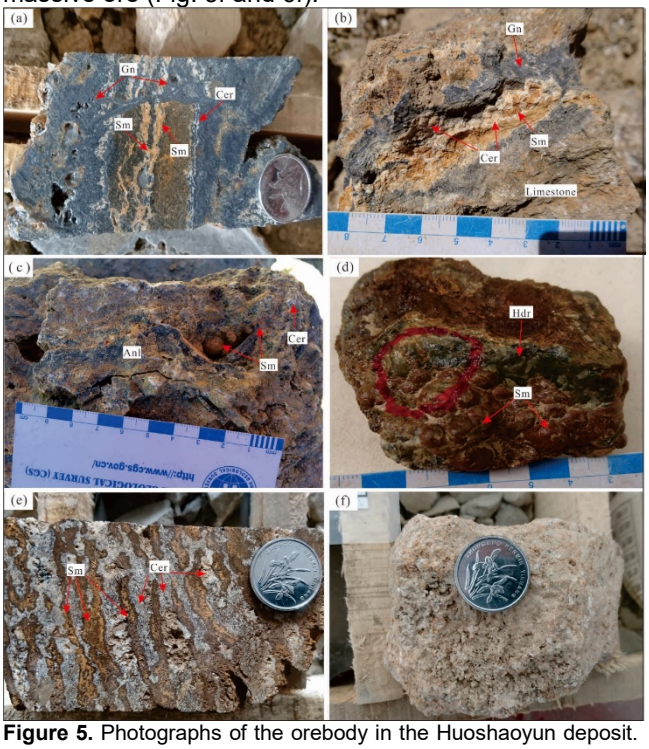

Figure 5. Photographs of the orebody in the Huoshaoyun deposit. (a) residual sulfide minerals after oxidation; (b) breccia matrix composed of disseminated cerussite and minor smithsonite; (c) black cerusite contains abundant relics of galena; (d) the smithsonite precipitates as massive botryoidal layers; (e) The nonsulphide zinc ore rhythmic replacement of cerusite and as joint fillings; (f) the massive ore consists of cerussite. Gn=galena, Sm=smithsonite, Cer=cerussite, Hdr=hydrozincite, Anl=anglesite.

During the oxidation and post-oxidation stages, oxidation, fractionation, and precipitation processes that formed the supergene nonsulphide ore, through a distinct progress of geochemical evolution. Moreover, the replacement textures between sulphide and non-sulphide ore at different scales, strongly suggest that the predominant mass of nonsulphide ore has been formed by in-situ oxidative leaching of the sulphide ore, multistage replacement and re-precipitation with weak metal fractionation or secondary zinc enrichment only.

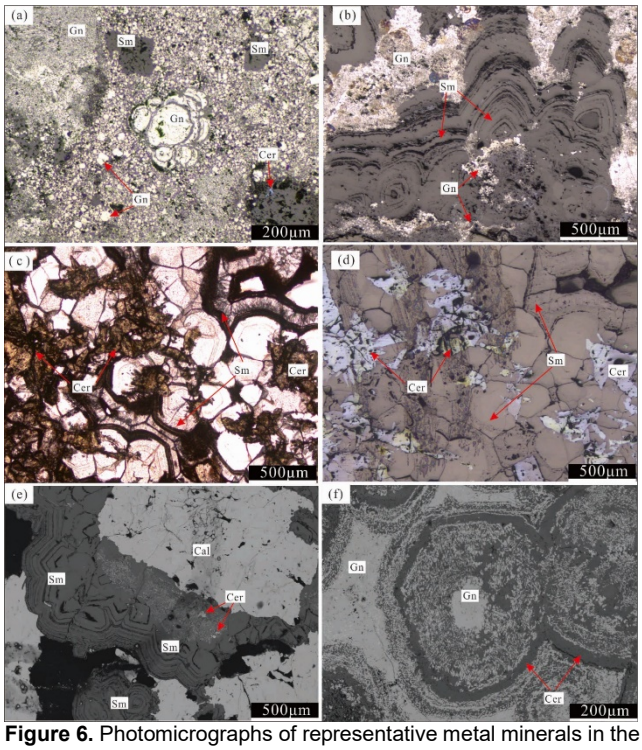

Figure 6. Photomicrographs of representative metal minerals in the Huoshaoyun deposit. (a) the galena is commonly rimmed by anglesite that contains abundant sub-size galena inclusions; (b) banded smithsonite in the post-oxidation stage; (c) and (d) cerussite and smithsonite under transmitted and reflected light; (e) banded smithsonite developed in the margin of calcite, in a backscattered electron image; (f) residual galena granule in the center of a circle of cerussite after oxidation. Gn=galena, Sm=smithsonite, Cer=cerussite, Cal=calcite.

3 Possible genetic type

The Zn-Pb mineralization in the Huoshaoyun deposit occurred at 26.6 ± 1.7 Ma (unpublished data), suggesting that metallogenesis of the Huoshaoyun deposit directly relates to the India-Eurasia collision. The late collision between the Indian plate and Eurasian plate happened at about 40~25 Ma based on the magmatic zircon results from north Tibet (Chung et al. 1998; Hou et al. 2006; Zhai et al. 2009). Before the Zn-Pb mineralization at Huoshaoyun, the Trassic-Jurassic limestone strata thickened and folded due to the large-scale regional thrusting. This not only provided favourable lithological and structural traps for fluids, but drove basin brines carrying ore-forming metals over a long distance. Therefore, the late Paleogene was a significant period for carbonate-hosted deposits. Such as Jinding deposit (Deng et al. 2017, Leach et al. 2016), Mohailaheng deposit (Liu et al. 2015, Liu et al. 2011), Duocaima deposit (Song et al. 2015), and this period is marked by a series of continental collisional events (Yin and Harrison, 2003; Deng et al., 2014a, 2014b).

Because there is no apparent genetic association with igneous activities, we classify the Huoshaoyun Zn-Pb deposit as a sediment-hosted Pb–Zn deposit. The Huoshaoyun deposit shows some syngenetic

characteristics that are typical of MVT deposits, e.g. host rock, mineralogy, alteration, deposit morphology, ore textures, temperature (Leach et al. 2005), although the Huoshaoyun deposit occurs in a compressional fold and thrust belt associated with the Tibetan plateau orogen, which is an unusual tectonic setting for MVT deposits (Liu et al. 2011). Different from other MVT Pb-Zn deposits in China, the geotectonic setting within the overriding plate of the active convergent plate of Tibet provided long term uplift, erosion, rapid exhumation of the sulphide protore, and exposure to oxygenated surface waters (Daliran and Borg 2005). Arid paleoclimatic conditions prevented the nonsulphide solutions from being flushed out of the system. Oxidation processes may have been additionally promoted by a regional high heat flow due to the young geothermal activities. Smithsonite and cerussite were probably formed by mixing of the CO^{2-} rich meteoric waters with the hydrothermal fluids. In all, we conclude that the Huoshaoyun deposit is a MVT deposit, which is a new discovered nonsulfide type in China.

Acknowledgements

This study was jointly supported by the National Key R & D Program of China (Grant No. 2018YFC0603704) and the Geological Survey Project of the China Geological Survey (DD20160050).

References

Rajabi A., Rastad E., Canet C. (2012). Metallogeny of Cretaceous carbonate-hosted Zn-Pb deposits of Iran: geotectonic setting and data integration for future mineral exploration. International Geology Review, 54:1649-1672

Chung S.-L.,Lo C.-H.,Lee T.-Y.,Zhang Y.,Xie Y.,Li X....Wang P.-L. (1998). Diachronous uplift of the Tibetan plateau starting 40 Myr ago. Nature, 394:769

Daliran F., Borg G. (2005). Characterisation of the nonsulphide zinc ore at Angouran, Northwestern Iran, and its genetic aspects. Mineral Deposit Research: Meeting the Global Challenge, Chapter 9-11.

Deng J.,Wang Q.,Li G., Santosh M. (2014a). Cenozoic tectono-magmatic and metallogenic processes in the Sanjiang region, southwestern China. Earth-Science Reviews, 138:268-299

Deng J.,Wang Q.,Li G.,Li C., Wang C. (2014b). Tethys tectonic evolution and its bearing on the distribution of important mineral deposits in the Sanjiang region, SW China. Gondwana Research, 26:419-437

Deng J.,Wang C.,Bagas L.,Selvaraja V.,Jeon H.,Wu B., Yang L. (2017). Insights into ore genesis of the Jinding Zn–Pb deposit, Yunnan Province, China: Evidence from Zn and in-situ S isotopes. Ore Geology Reviews, 90:943-957.

Deng J.Q., Lin Y.X. (2015). Propagation of the deformation and growth of the Tibetan-Himalayan orogen: A review. Earth-Science Reviews, 143:36-61

Dong L.H., Xu X.W., Fan T.B., Qu X., Li H., Liu C. (2015). Discovery of the Huoshaoyun Super-Large Exhalative-Sedimentary Carbonate Pb-Zn Deposit in the Western Kunlun Area and its Great Significance for Regional Metallogeny. Xinjiang Geology, 33(1):41-50 (in Chinese with English abstract).

Hou Z.Q, Pan G.T, Wang AJ., Mo X.X, Tian S.H, Sun X.M, Ding L, Wang E.Q, Gao Y.F, Xie Y.L, Zeng P.S, Qin K.Z, Xu J.F, Qu X.M, Yang Z.M, Yang Z.S, Fei H.C, Meng X.J and Li Z.Q. (2006). Metallogenesis in Tibetan collisional orogenic belt: II. Mineralization in late collisional transformation setting. Mineral Deposits, 25(5):521-544 (in Chinese with English abstract)

Hou ZQ, Song YC, Li Z, Wang ZL, Yang ZM, Yang ZS, Liu YC, Tian SH, He LQ, Chen KX, Wang FC, Zhao CX, Xue WW and Lu HF. (2008). Thrust-controlled, sediments-hosted Pb-Zn-Ag-Cu deposits in eastern and northern margins of Tibetan orogenic belt: Geological features and tectonic model. Mineral Deposits, 27(2):123-144 (in Chinese with English abstract)

Hou Z.,Zhang H.,Pan X., Yang Z. (2011). Porphyry Cu (–Mo–Au) deposits related to melting of thickened mafic lower crust: Examples from the eastern Tethyan metallogenic domain. Ore Geology Reviews, 39:21-45

Leach, D., Bradley, D., Huston, D., Pisarevsky, S., Taylor, R., Gardoll, S. (2010). Sediment-hosted lead-zinc-deposits in earth history. Economic Geology, 105(3):593-625.

Leach D.L.,Song Y.C., Hou Z.Q. (2016). The world-class Jinding Zn–Pb deposit: ore formation in an evaporite dome, Lanping Basin, Yunnan, China. Mineralium Deposita, 52:1-16

Liu Y.C.,Yang Z.S.,Tian S.H.,Song Y.C., Zhang H.R. (2015). Fluid origin of fluorite-rich carbonate-hosted Pb–Zn mineralization of the Himalayan–Zagros collisional orogenic system: A case study of the Mohailaheng deposit, Tibetan Plateau, China. Ore Geology Reviews, 70:546-561

Liu Y.C, Hou Z.Q, Yang Z.S, Tian S.H, Yang T.N, Song Y.C, Carranza E.JM. (2011). Formation of the Dongmozhazhua Pb–Zn Deposit in the Thrust‐Fold Setting of the Tibetan Plateau, China: Evidence from Fluid Inclusion and Stable Isotope Data. Resource Geology, 61:384-406

Mirnejad H., Simonetti A., Molasalehi F. (2011). Pb isotopic compositions of some Zn–Pb deposits and occurrences from Urumieh–Dokhtar and Sanandaj–Sirjan zones in Iran. Ore geology reviews, 39:181-187

Song Y.,Yang T.,Zhang H.,Liu Y.,Hao H., Li Z. (2015). The Chaqupacha Mississippi Valley-type Pb–Zn deposit, central Tibet: Ore formation in a fold and thrust belt of the India–Asia continental collision zone. Ore Geology Reviews, 70:533-545

Spurlin M.S.,Yin A.,Horton B.K.,Zhou J., Wang J. (2005). Structural evolution of the Yushu-Nangqian region and its relationship to syncollisional igneous activity, east-central Tibet. Geological Society of America Bulletin, 117:1293-1317

Yin A., Harrison T.M. (2003). Geologic Evolution of the Himalayan-Tibetan Orogen. Annual Review of Earth & Planetary Sciences, 28:211-280

Zhai Q G, Li C, Wang J, Chen W. (2009), $^{40}Ar/^{39}Ar$ dating for Cenozoic potassic volcanic rocks in northern Gemucuo from Qiangtang, northern Tibet, China. Geological Bulletin of China, 28(9):1221-1228.